Supplement of Geosci. Model Dev., 12, 2707–2726, 2019
https://doi.org/10.5194/gmd-12-2707-2019-supplement

Geoscientific Model Development
Open Access
EGU

Supplement of

Modeling extreme precipitation over East China with a global variable-resolution modeling framework (MPASv5.2): impacts of resolution and physics

Chun Zhao et al.

Correspondence to: Yu Wang (wangyu09@ustc.edu.cn)

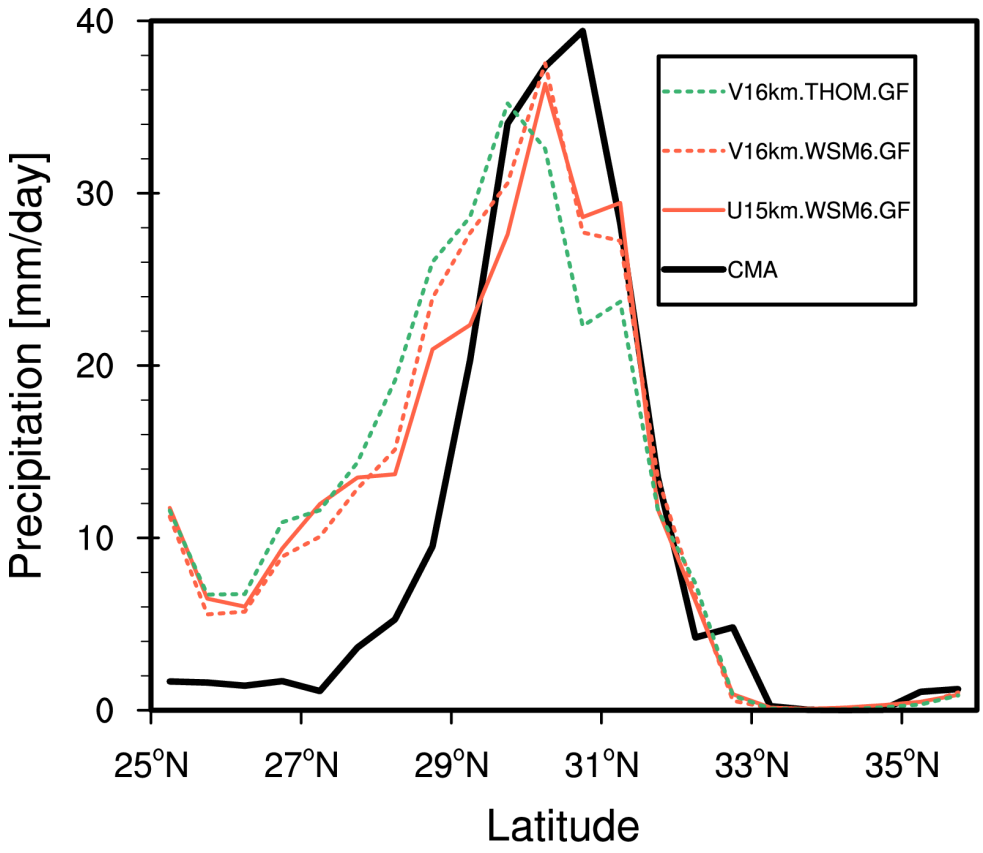

Figure S1 Zonal distributions of precipitation averaged during the event (June 25 00:00 to June 27 12:00 UTC time) over East China (denoted as the black box in Fig. 2) from the CMA station observations and the simulations with the global uniform (15 km, solid lines) and variable (16 km over the refined region as shown in Fig. 1c, dash lines) resolutions with two cloud microphysics parameterizations (WSM6, red dash lines; Thompson, green dash lines). The modeling results are sampled at the CMA station.

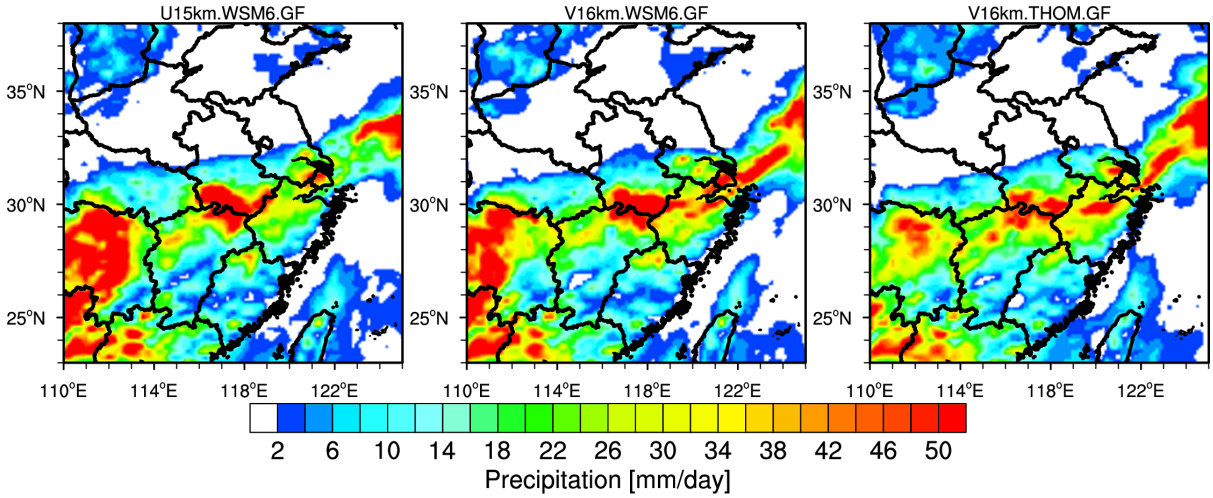

Figure S2 Spatial distributions of precipitation averaged during the event (June 25 00:00 to June 27 12:00 UTC time) from the simulations with the global uniform (15 km) and variable (16 km over the refined region as shown in Fig. 1c) resolutions. The V16km simulations with the WSM6 and Thompson cloud microphysics schemes are shown. The spatial correlation coefficient between the V16km simulations with two different cloud microphysics is 0.85.

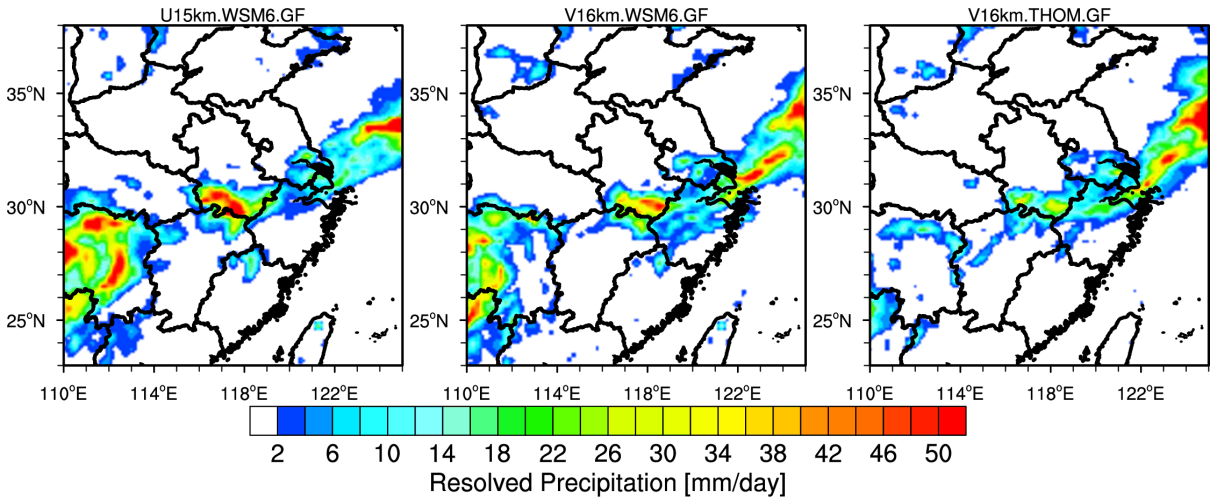

Figure S3 Spatial distributions of grid-resolved precipitation averaged during the event from the simulations with the global uniform (15 km) and variable (16 km over the refined region) resolutions. The V16km simulations with the WSM6 and Thompson cloud microphysics schemes are shown. The spatial correlation coefficient between the V16km simulations with two different cloud microphysics is 0.

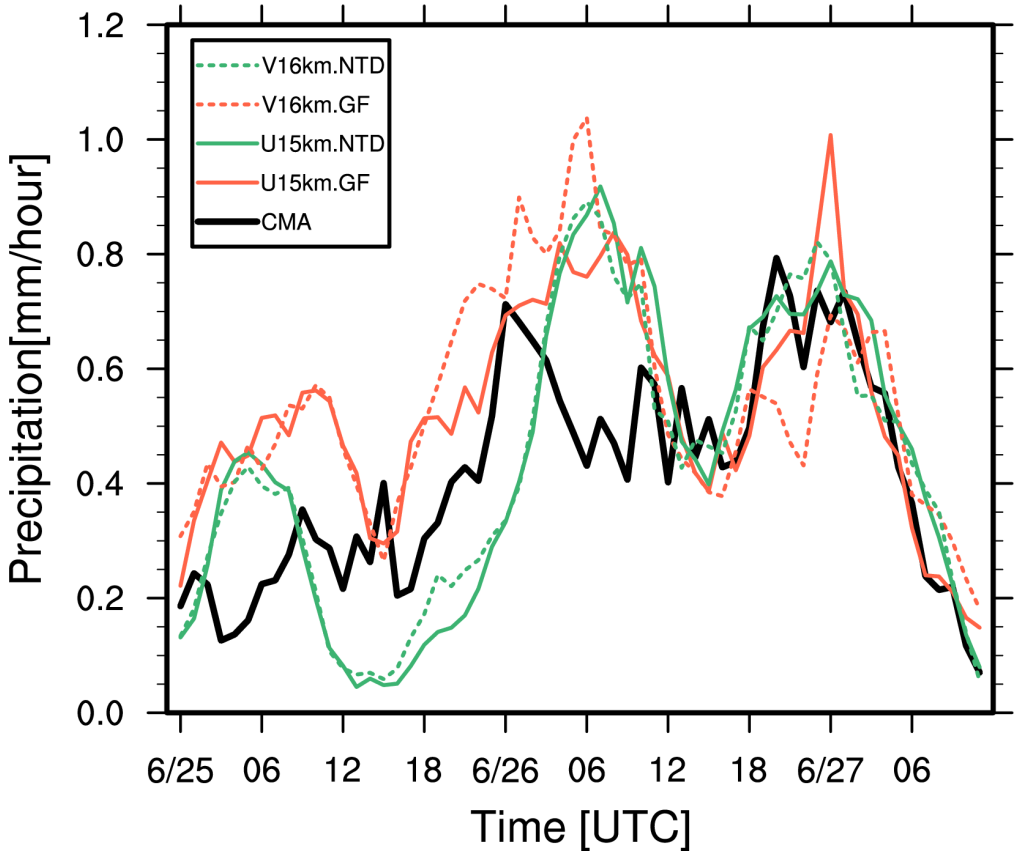

Figure S4 Temporal variation of precipitation during the event averaged over East China (denoted as the black box in Fig. 2) from the CMA station observations and the simulations with the global uniform and variable resolutions with two convective parameterizations. The modeling results are sampled at the CMA stations.

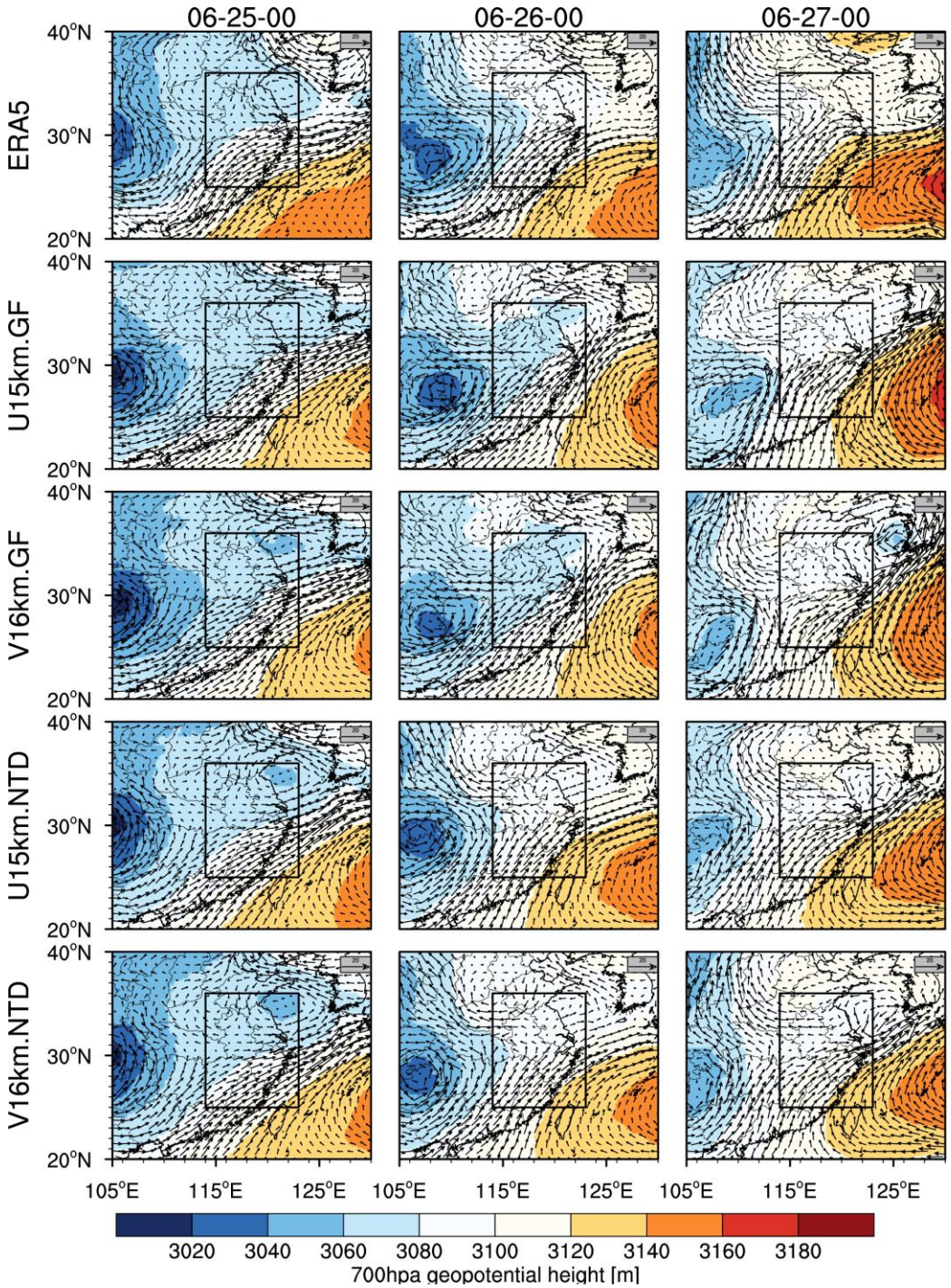

Figure S5 Spatial distributions of geopotential height and wind fields at 700 hPa at UTC 0000 of each day during the simulation (June 23 00:00 to June 27 00:00 UTC time) from the simulations with the global uniform (15 km) and variable (16 km over the refined region as shown in Fig. 1c) resolutions. The black box denotes the region for the analysis in this study.

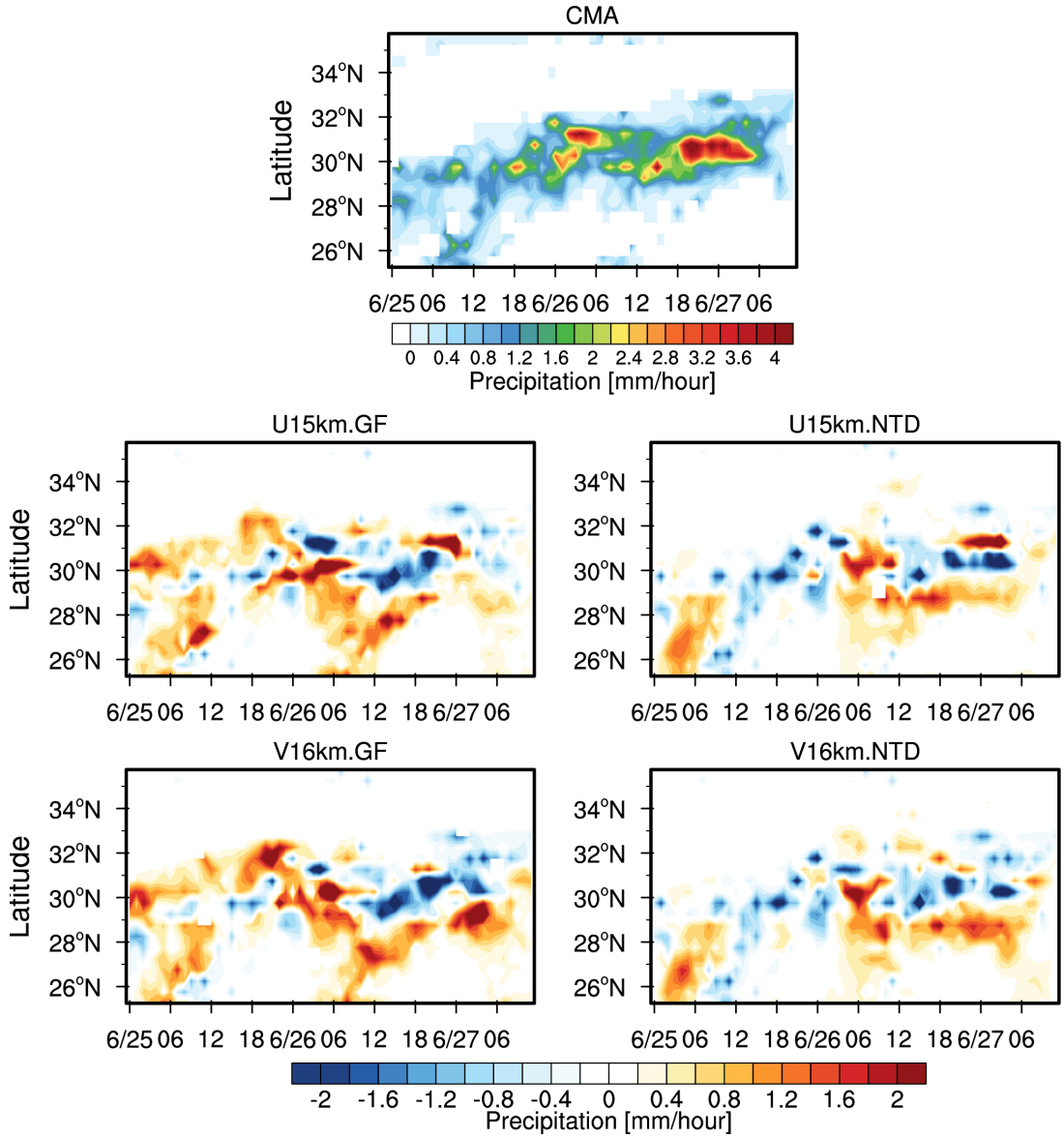

Figure S6 Time-Latitude cross section of precipitation during the event over East China from the CMA station observations and difference between the CMA and the simulations (simulation minus observation) with the global uniform and variable resolutions with two convective parameterizations. The modeling results are sampled at the CMA stations.

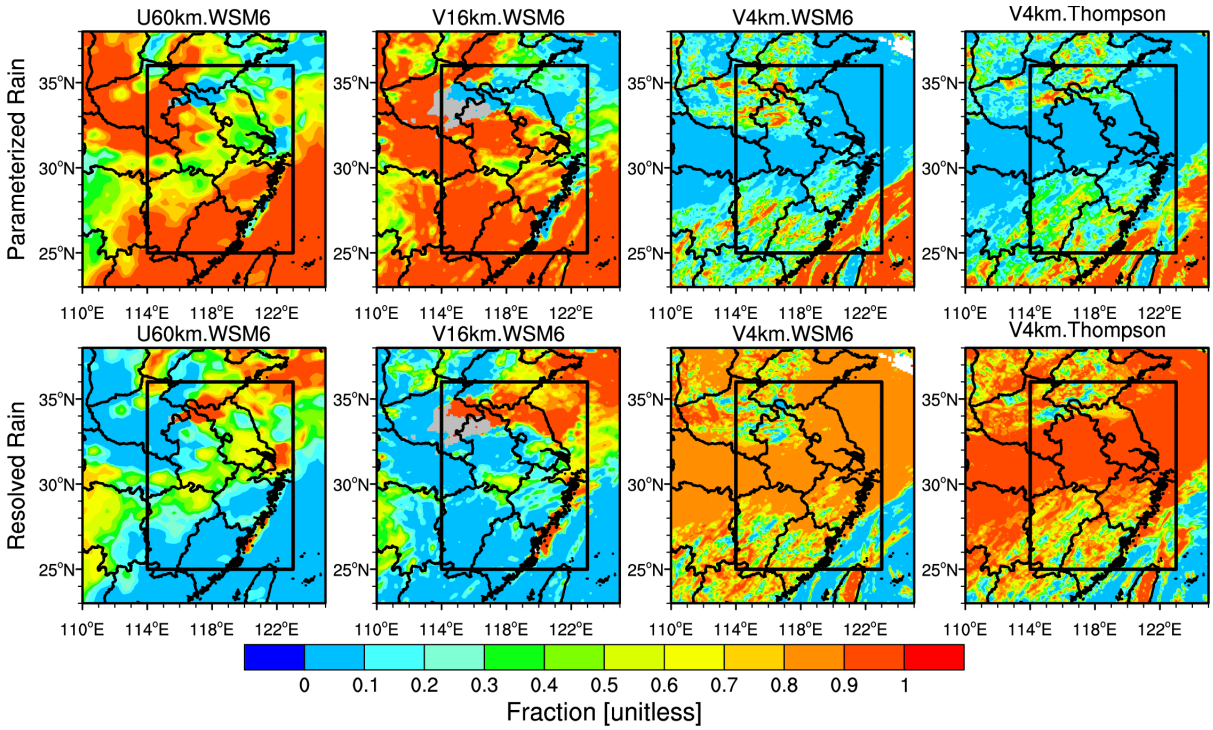

Figure S7 Spatial distribution of fraction of averaged parameterized and resolved precipitation in total precipitation during the event over East China from the simulations with the resolutions of 60 km, 16 km, and 4 km.

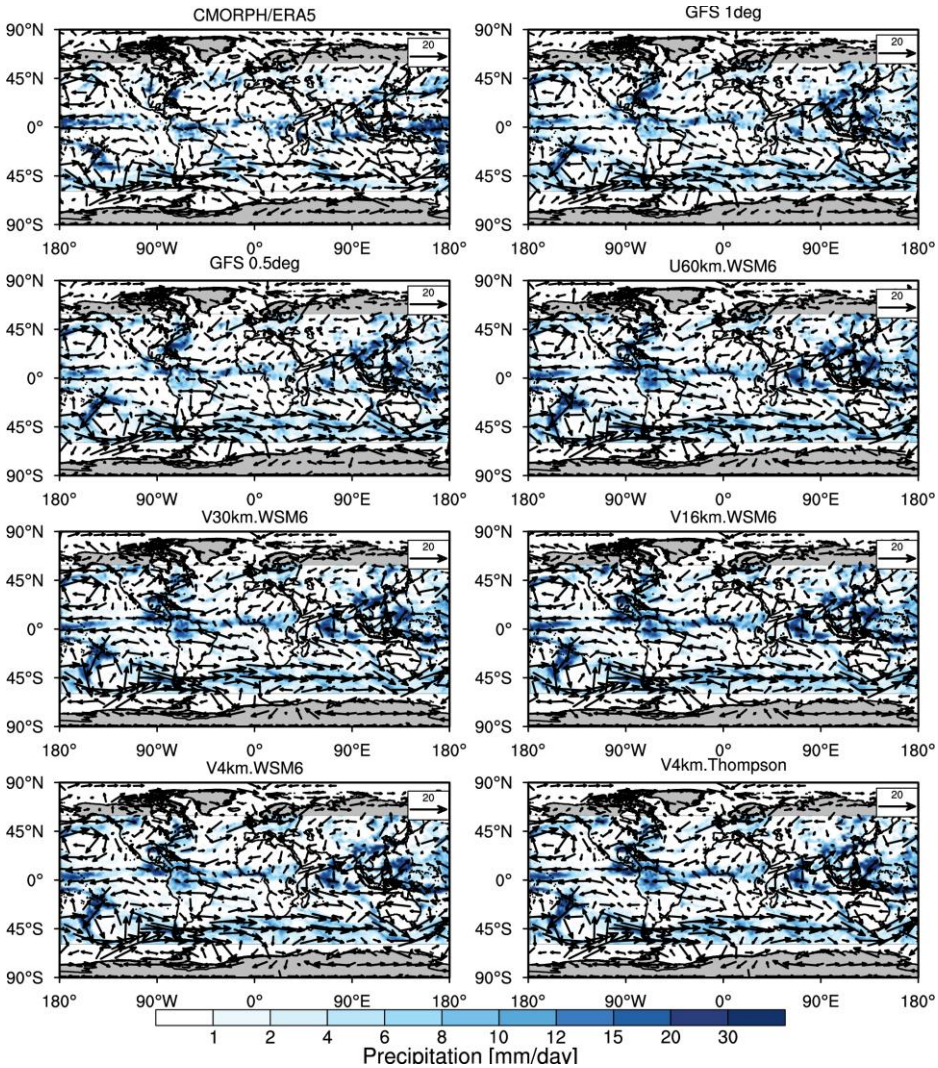

Figure S8 Global distributions of precipitation and wind fields at 850 hPa averaged during the event from the MPAS simulations at the resolutions of U60 km, V30 km, V16 km, and V4 km. The observed mean precipitation from the CMORPH satellite retrievals (downloaded from https://climatedataguide.ucar.edu/climate-data/cmorph-cpc-morphing-technique-high-resolution-precipitation-60s-60n) and the wind fields from the ERA5 reanalysis are shown as well. The black box denotes the region for the analysis in the following. For comparison, the GFS forecasts at 1 degree and 0.5 degree resolutions are also shown.

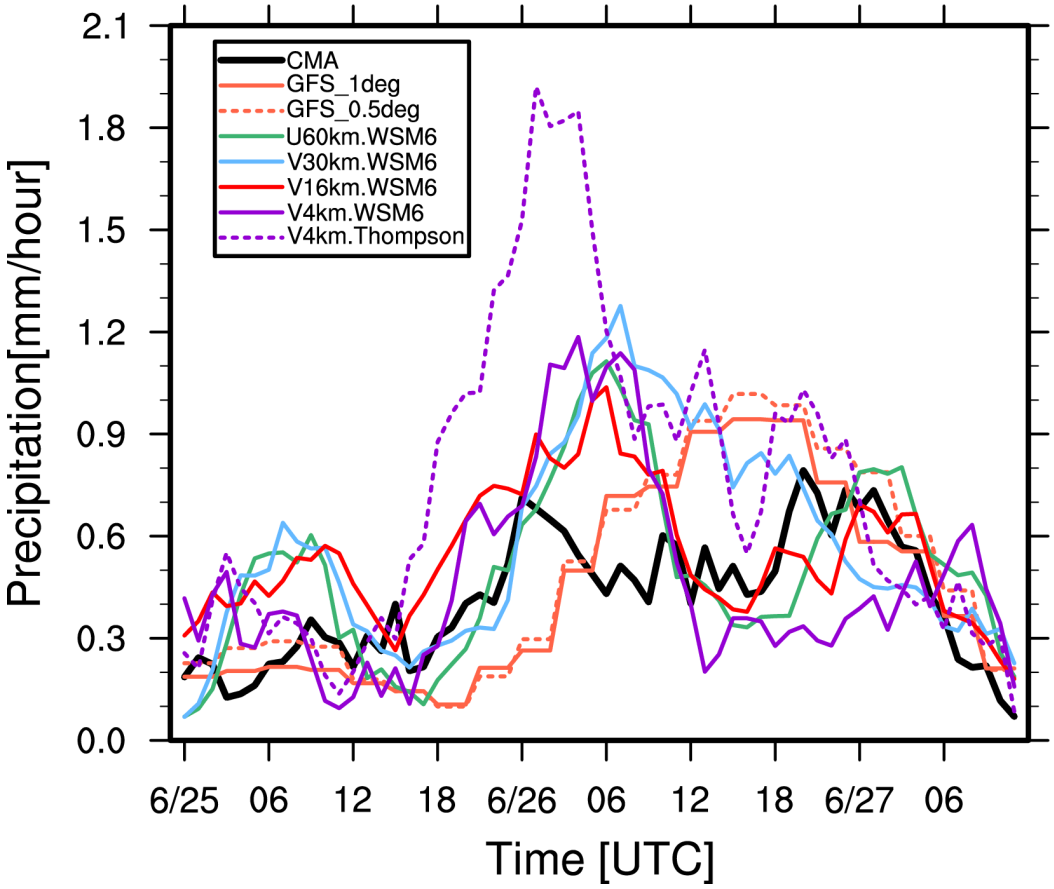

Figure S9 Temporal variation of precipitation during the event averaged over East China (denoted as the black box in Fig. 2) from the CMA station observations, the GFS forecasts, and the MPAS simulations at multiple resolutions and with two cloud microphysics parameterizations. The modeling results are sampled at the CMA stations.

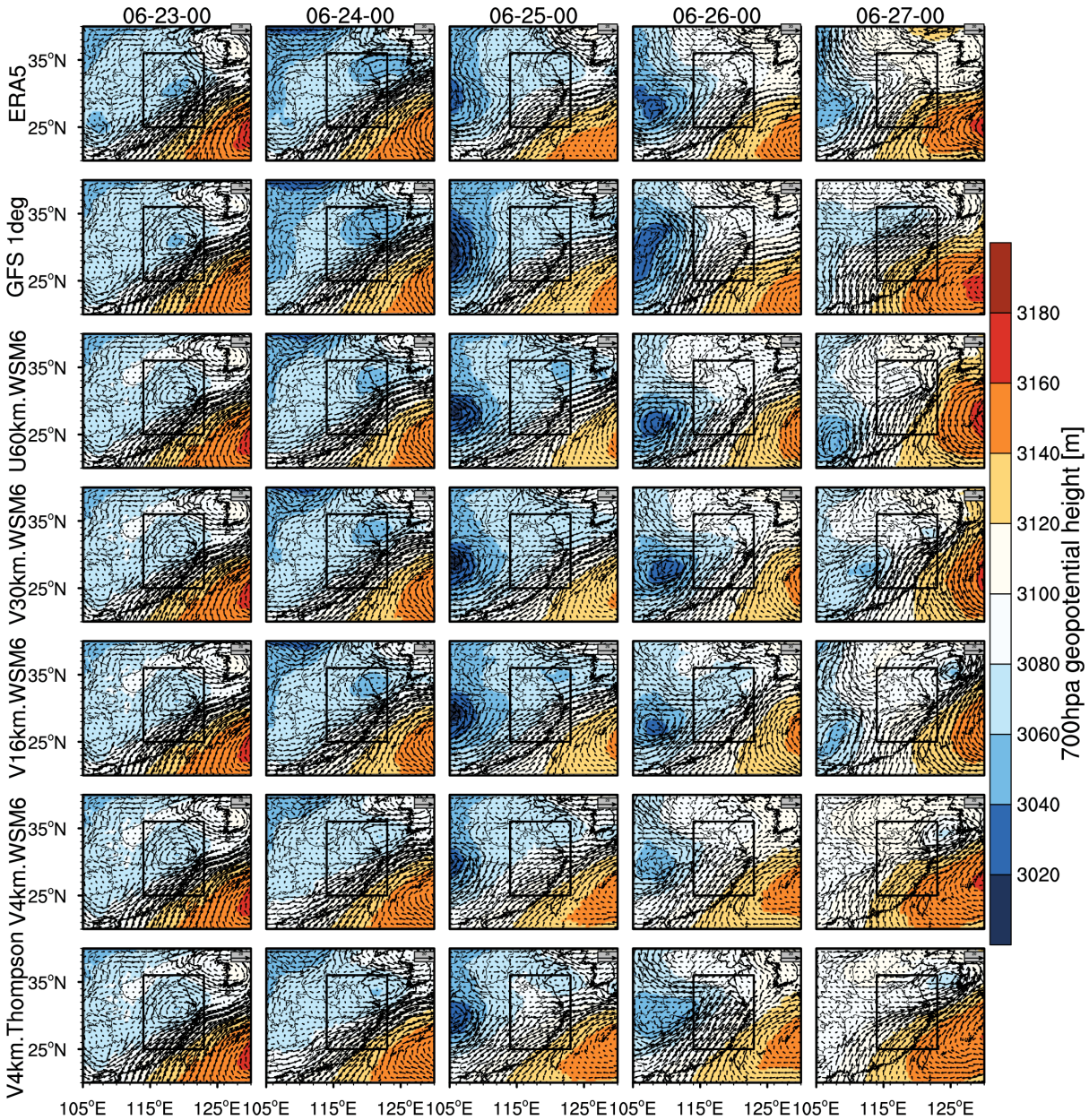

Figure S10 Spatial distributions of geopotential height and wind fields at 700 hPa at UTC 0000 of each day during the simulation (June 23 00:00 to June 27 00:00 UTC time) from the MPAS simulations at the resolutions of 60 km, 30 km, 16 km, and 4 km. The black box denotes the region for the analysis in this study. For comparison, the GFS forecast at 1 degree resolution is also shown.

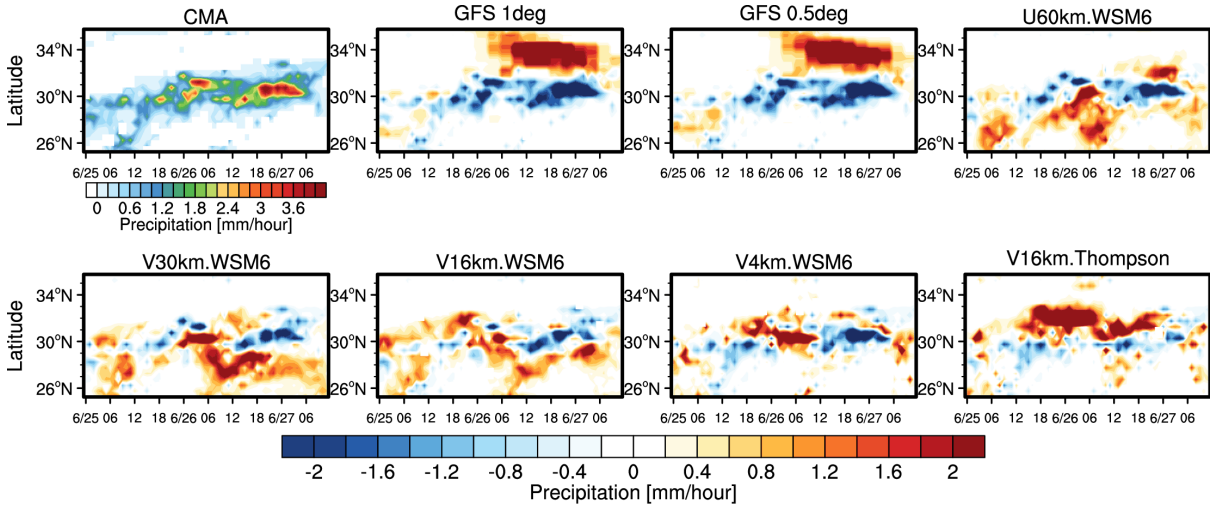

Figure S11 Time-Latitude cross section of precipitation during the event over East China from the CMA station observations and difference between the CMA and the GFS forecasts, the MPAS simulations (simulation minus observation) at multiple resolutions and with two cloud microphysics parameterizations. The modeling results are sampled at the CMA stations.